A versatile electrode sorting module for MEAs: implementation in a FPGA-based real-time system

Antoine Pirog, Yannick Bornat, Sylvie Renaud, Romain Perrier, Manon Jaffredo, Matthieu Raoux, Jochen Lang

A versatile electrode sorting module for MEAs: implementation in a FPGA-based real-time system

Antoine Pirog, Yannick Bornat, Sylvie Renaud
IMS, Univ. Bordeaux, Bordeaux INP, CNRS UMR 5218
F-33400 Talence, France
antoine.pirog@ims-bordeaux.fr

Romain Perrier, Manon Jaffredo, Matthieu Raoux, Jochen Lang
CBMN, Univ. Bordeaux, CNRS UMR 5248
F-33600 Pessac, France

***Abstract*—Extracellular recordings of biological signals using Multi-Electrode Arrays (MEAs) generate large quantities of multichannel data which are not all relevant. Indeed, cultured cells might not cover all electrodes or achieve sufficient electrical contact. In both bench experiments and implant-oriented devices, it is necessary to identify such defects and exclude corresponding electrodes from the processing pool. In the context of a real-time, FPGA-based multichannel signal processing system, this paper presents a versatile electrode sorting module. It uses low-complexity, user-configurable algorithms and supports synchronization, frequency, and amplitude criteria, as well as definable inclusion/exclusion rules. This module relieves the experimenter from constantly monitoring unusual behavior and promotes automatization. The module's efficacy was demonstrated during *in vitro* experiments on noise-prone pancreatic islets.**

Keywords—FPGA, Multi-Electrode Array, electrode sorting, biosignals, real-time, pancreatic islets

I. INTRODUCTION

Contemporary electrophysiology research, often related, but not limited to neurosciences, has built an immense interest in networks of cells. While long-established techniques, such as patch-clamp, could only focus on a limited number of cells, advances in electrode technology have brought new tools to investigate the group behavior of whole clusters of cells. Multi-electrode arrays (MEA) are matrices of tens to hundreds of non-invasive electrodes that capture a change in voltage caused by the ion currents in the vicinity of an excitable cell [1][2], such as neurons, muscle cells, and some endocrine cells (e.g. pancreatic α- and β-cells). They can either be used *in vitro*, to facilitate the study of networks of cells, or *in vivo*, to investigate neuroprosthetics or retinal prosthetics [3].

Signals recorded with extracellular electrodes present typical signatures, as illustrated in Fig. 1A. These include the widely-described Action Potentials (APs or spikes), a fast-pulsing activity (a few milliseconds) generated by a single cell. APs often appear in bursting patterns, where a fast (>10 Hz) succession of APs is fired during a limited period, usually associated with a Local Field Potential (LFP). On a larger scale, micro-organs, such as the pancreatic islets, composed of hundreds of excitable cells, display continuous oscillations, reflecting cell coupling. These Slow Potentials (SPs) have frequency components ranging below 1 Hz [4].

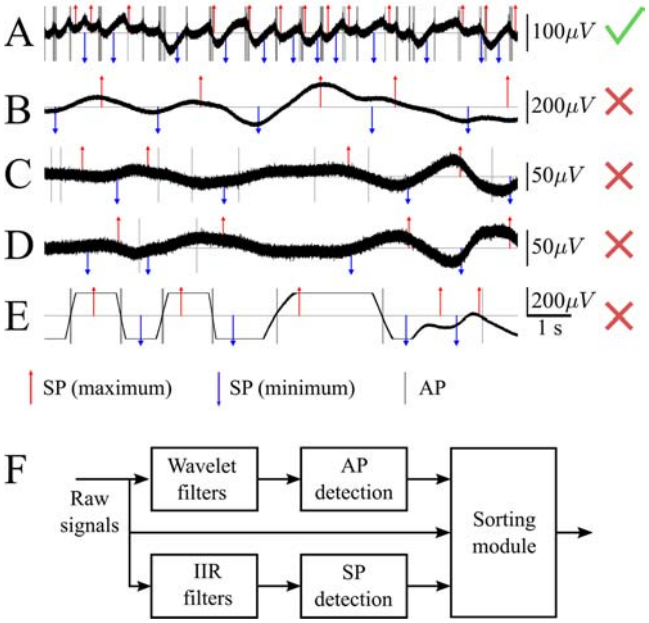

Fig. 1. Typical signals, inputs, and environment of the electrode sorting module. **A** to **E**: Typical signals recorded on a pancreatic islet preparation cultured in MEAs, and their corresponding AP and SP maxima and minima event detection. Note that SP maxima and minima timestamps include filtering delay. **A**: A valid signal in excitatory conditions, featuring both APs and SPs. **B**: An invalid signal featuring low frequency, abnormal oscillations in inhibitory conditions. **C** and **D**: Coupled signals, indicative of an electrical contact issue. **E**: A saturating signal, prone to cause processing errors. **F**: Processing environment of the sorting module. AP and SP events need to be detected prior to sorting.

MEAs are versatile tools, with various uses and applications in electrophysiology. They provide multisite, real-time readouts of cell activity with the potential for network analysis with high time resolution, but generally lack spatial resolution. The chances of having a cell within measuring distance remain slim, considering the small active surface and electrode sparsity (typically, electrode diameter is 10% of electrode spacing). Increasing electrode coverage necessitates an upscale in the number and density of electrodes, cell-guiding techniques [5], or dedicated topologies [2]. Even then, the proportion of covered and exploitable electrodes never reaches 100%. In chronic recordings, the apparition of fibroblasts and scar tissue systematically results in additional electrode loss [6]. Moreover, multiple sources for hardware failure exist in the acquisition chain, from the MEA itself to the

978-1-5090-5803-7/17/$31.00 ©2017 IEEE

multichannel amplifier and the mechanical spring-loaded contacts between them.

These issues usually result in unnecessary processing of uncovered electrodes. To address this important issue, we developed a digital module, inspired from experiments, to sort and automatically constitute a set of normally-behaving electrodes. This module is part of a VHDL architecture dedicated to biosignal processing. The necessary environment for the sorting module is represented in Fig. 1F.

The present work was developed within the context of measuring pancreatic β-cell and islets of Langerhans on planar MEAs, in which exocrine tissue is often a source for deterioration of both electrode coverage and signal quality. This module automates the process of detecting unusual behavior to later include or exclude electrodes from the online- and post-processing pools.

II. ALGORITHMS

The general methodology adopted to define a set of valid electrodes is to exclude electrodes that are responsive in inhibitory conditions (Fig. 1B), and include those that display a physiological response in excitatory conditions (Fig. 1A). The physiological characteristic of the response is determined by the experimenter and is usually related to both the frequency and amplitude of the measured events (in the context of pancreatic islets APs and SPs). Finally, the electrodes that present an electronic malfunction, such as coupling (Fig. 1C-D) or saturation (Fig. 1E) are excluded as well.

The module sorts electrodes based on raw signals and events, detected by upstream modules (represented in Fig. 1F but not described in this paper). The sorting algorithms discriminate electrodes based on any or all of (a) their event frequencies, (b) synchronous activity, and (c) signal amplitude.

Event frequency is obtained by counting events over a limited period of time T. An electrode is flagged active if this count exceeds a threshold as described in equation (1) below:

$$\begin{cases} a_n^i = \min(a_{n-1}^i + x_n^i, \Delta) \\ A^i = \begin{cases} 1, & a_N^i = \Delta \\ 0, & a_N^i < \Delta \end{cases} \end{cases} \quad (1)$$

Where $n = 1 \dots N$ is the current sample number, a_n^i is the n^{th} value of the event counter of electrode i, x_n^i is the n^{th} input of the event counter of electrode i (either 1 if an event is present or 0 otherwise), Δ is the event threshold, N is the total number of samples over T and A^i is the activity flag for channel i.

Detection of synchronization between electrodes is based on a leaky event counter. For each electrode, incoming events increase a counter s by a step ε_U. Otherwise, the counter decreases by a step ε_D at every T/N. This gives each event a weight that decreases with time. If the sum of all counters exceeds a threshold Q, meaning that a sufficient amount of events were fired in a short time window, a synchronization event S is fired, related to all involved electrodes. This process is summarized in equation (2) below:

$$s_n^i = \begin{cases} 0, & \sum_{i' \in I} s_{n-1}^{i'} + x_n^{i'} \times \varepsilon_U \geq Q \\ \max(s_{n-1}^i + x_n^i \times \varepsilon_U - \varepsilon_D, 0), & \text{otherwise} \end{cases} \quad (2a)$$

$$S_n^i = \begin{cases} 1, & \sum_{i' \in I} s_n^{i'} \geq Q \text{ and } s_n^i > 0 \\ 0, & \text{otherwise} \end{cases} \quad (2b)$$

Where n is the current sample number, s_n^i is the n^{th} value of the event counter of electrode i, x_n^i is the n^{th} input of the event counter of electrode i (either 1 if an event is present or 0 otherwise), S_n^i is the n^{th} synchronization event of electrode i, and I is the set of all electrodes. In order to detect repeated synchronization only and avoid false positives, the synchronization events S_n^i are then processed by the algorithm described in (1).

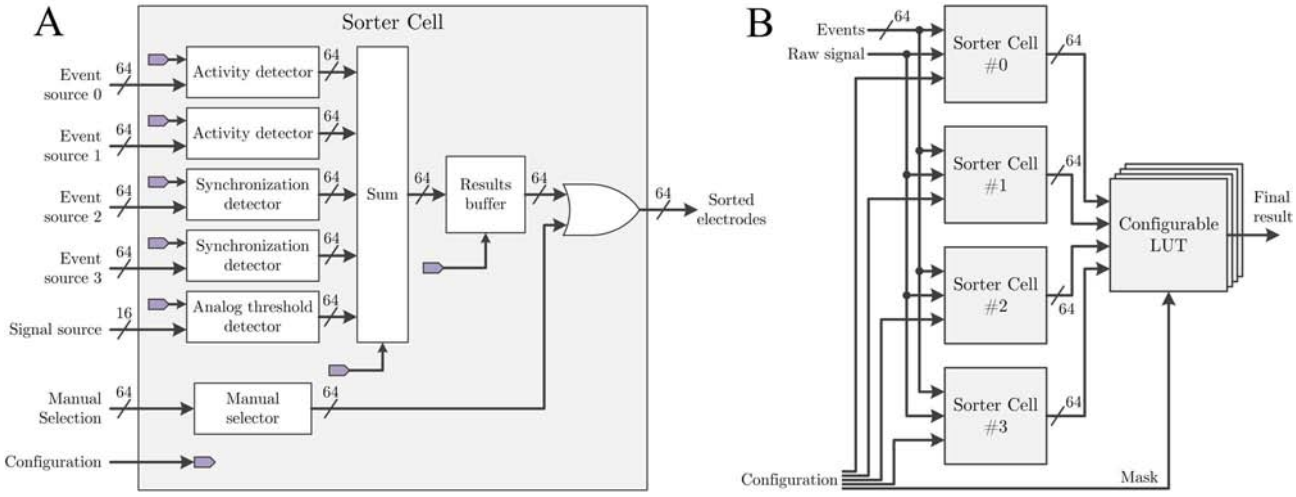

Fig. 2. Architecture of the electrode sorting module. **A**: Architecture of a single sorting cell. **B**: architecture of the complete module, with four sorting cells and a configurable LUT.

Finally, sorting electrodes according to amplitude criteria is simply achieved by comparing the signal value to a definable threshold. If the input sample exceeds it, the corresponding electrode is flagged.

In order to recreate the methodology of the experimenter, the event-based algorithms are duplicated to be used for both APs and SPs, and the ensemble of all algorithms, forming one sorter cell (Fig. 2A), is duplicated four times (Fig. 2B) to permit different configurations and intermediary results. The final sorting result is any logic combination of all four intermediary results (intermediary and final results are accessible for readout), representing experimenter-defined inclusion/exclusion rules.

III. Implementation and Architecture

The module in Fig. 2B is part of a multichannel, real-time processing VHDL architecture. The system is designed to extract events and perform measurements on excitable cells cultured in planar MEAs. In this paper the system was used to measure pancreatic islets cultured in 60-electrodes MEAs.

The module's input/output communication schemes are defined as follows: Multichannel event data is a 65-bit parallel bus including 64 event bits (60 from electrode processing and 4 dummy channels for tests) and an enable bit. Events in the system are sampled at 1 kHz. Multichannel raw signals, sampled at 10 kHz, are transferred as pipelined data bursts on a 17-bit bus with one start bit and 16 data bits at a rate of one channel per clock cycle.

These communication rules motivated parallel computation schemes for event-based computation (activity detector, synchronization detector, summing, and buffering modules in Fig. 2A) and fully pipelined schemes for signal-driven modules (analog threshold detector in Fig. 2A).

Each sorter cell, represented in Fig. 2A, contains two 64-input activity detectors, two 64-input synchronization detectors, and a pipelined analog threshold detector. A summing module performs a logical OR on a configurable selection of all detector results, meaning that some sorting criteria can be bypassed. The summing module waits for all its used detectors to transmit their results, sums them and sends the result to a buffer. This buffer can be controlled to either overwrite its contents or sum new results. It contains the sorter cell result in a 64-bit memory. Alongside this automatic detection chain, a manual electrode selector provides the experimenter the possibility to force inclusions or exclusions. The set of manually flagged electrodes is added to the contents of the result buffer, and the experimenter may either exclusively sort electrodes manually, add complementary information to automatic sorting, or leave manual sorting blank.

The complete sorting module is composed of four identical sorter cells, as shown in Fig. 2B. A dynamically configurable LUT (Lookup Table) was implemented to define the overall inclusion/exclusion rule. To accommodate for parallel communication rules, the LUT is a group of 64 4:1 LUTs with a unique mask.

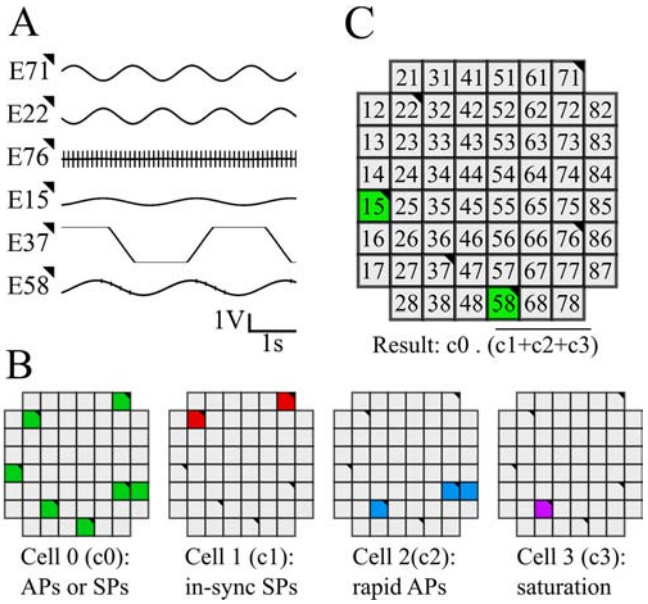

Fig. 3. Validation of sorting algorithms on test signals, applied on six electrodes marked on the MEA matrix with black corners. **A**: Test signals used. E71 and E22 were 0.8 Hz, 0.9 Vpp sine waves in phase opposition. E76 was a 10 Hz continuous burst of 0.9 Vpp biphasic pulses. E15 was a 0.5 Hz, 200 mVpp sine wave. E37 was a 0.3 Hz, 4 Vpp sine wave, clipped at ±1 V by the input converters. E58 was a 0.5 Hz, 0.8 Vpp sine wave with bursts of 5 Hz pulses on the descending phase of the sine wave. **B**: Intermediary sorting results returned by the module on four sorting cells. Cell 0 flagged electrodes that had more than 30 APs or 3 SPs in 30 s. Cell 1 flagged electrodes that had 7 synchronized SPs within a 20 ms window in 10 s. Cell 2 flagged electrodes that had 100 APs or more in 10 s. Note that electrode 86 was flagged due to crosstalk with electrode 76 and electrode 37 was flagged because its saturation caused multiple AP detections. Cell 3 flagged electrodes which signal saturated. **C**: Final sorting result returned by the module. The LUT was configured to flag electrodes that had APs or SPs, did not have synchronized SPs, did not have unphysiological AP firing, and which signals did not saturate, hence the logical equation: $c0.\overline{(c1 + c2 + c3)}$. The two remaining electrodes (E15 and E58) are indeed the only two normally-behaving electrodes.

The sorting module is entirely configurable while in operation. Each parameter is an FPGA block input, handled as any other signal in the processing chain. A global configuration manager addresses 16-bit configuration words including a 5-bit address and 11 configuration bits to the corresponding parameter. Within a sorter cell, the accessible parameters include (a) event thresholds for both activity detectors (Δ in (1)), (b) increase and decrease steps (ε_U and ε_D in (2a)), (c) counter threshold (Q in (2b)), (d) synchronization event thresholds (Δ in (1)) for both synchronization detectors, and (e) a signal threshold for the analog threshold detector. As mentioned above, the experimenter may also configure the summing block to set which sorting criteria are used, and define whether the results buffer should overwrite or sum results at each new measurement. Finally, configuration includes an enable control and a buffer clear control. All these parameters are separately accessible for each sorter cell.

The sorting module was implemented on a Xilinx Spartan-6 FPGA, within an existing architecture dedicated to the processing of pancreatic islet signals. In isolation, the module uses 7425 slice registers (4% of available registers), 7068 LUTs (7% of available LUTs), and can operate at a maximum

clock frequency of 173.579 MHz. This amounts to a logic utilization of 116 (0.06%) slice registers and 1767 (0.1%) LUTs per electrode. The pipelined and parallel architecture reduces computation cost to linear algorithmic complexity, processing latency, and implementation cost.

IV. Tests and Validation

The sorting module was tested using synthetic signals to validate its function. It was placed in the processing chain of Fig. 1F, which includes AP and SP detection. Signals are calibrated to ensure 100% event detection rates prior to sorting. They were generated to feature the typical signatures represented in Fig. 1A-E and evoke similar event detection. This included low-frequency (0.3-0.8 Hz) sinewaves and fast (5-10 Hz) biphasic pulses. The signals were chosen to demonstrate and validate each sorting criterion, i.e. two synchronized signals, a fast pulsing signal, a saturating signal, and two valid. As represented in Fig. 3B-C, the sorting paradigm included all four sorting cells. Cell #0 detected electrodes with either AP or SP activity, cell #1 detected synchronized SPs, cell #2 detected rapid pulsing, and cell #3 detected saturation. The inclusion/exclusion rule stated that electrodes with SP or AP activity were included and electrodes with synchronization, excessive AP firing, or saturation were excluded. The sorting module successfully detected the two "normally-behaving" electrodes (Fig. 3C), and all sorting cells accurately detected electrodes meeting their criteria (Fig. 3B).

V. Results and Discussion

The sorting module was tested and used on pancreatic islets preparations (Fig. 4). The inclusion rule of the module stated that electrodes with more than 10 SPs in 60 s in excitatory conditions were retained. The exclusion rule rejected electrodes with either more than 5 SPs in 60 s or a peak amplitude of more than 300 µV in inhibitory conditions. One experimenter manually sorted electrodes, following the routine methodology, while another ran the sorting module, blinded from experimental observations. In Fig. 4, we compared both methods, manual sorting being the reference. In three experiments, the sorting module detected from 73% to 95% of valid electrodes. False detections were biased towards false negatives rather than false positives. This means that the detected subset of electrodes, though incomplete, is suitable for valid measurements and few (4%) electrodes are disruptive.

This sorting module recreates the methodology the experimenter adopts to include or exclude electrodes from an analysis pool. The module's purpose is to automate this process and generate a list of electrodes of interest for post-processing. This allows to optimize computing resources and storage space in a real-time multichannel processing environment. Coupled to a continuous control environment that periodically refreshes the measurement, it could improve system reliability, help to manage resources, and report on electrode loss in chronic experiments.

Acknowledgements

This work was supported by the French ANR-DGOS grant ISLET-CHIP (ANR 2013-PRTS-0017).

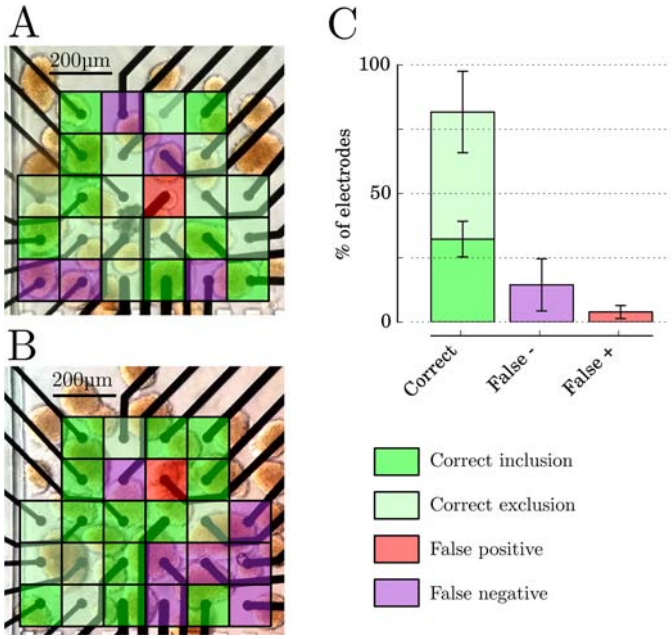

Fig. 4. Sorting results on N=3 different experiments. **A** and **B**: detection results overlayed with a photography of the preparation. **C**: repartition of electrode sorting results. On average, the module detected 4% false positives, 14% false negatives, and 82% correct detections.

VI. Conclusion

This communication proposes a VHDL implementation of an electrode sorting module for MEA recordings. It is inspired from experimental recordings involving activity, synchronization, and amplitude discrimination. The sorting criteria can be used in separate experimental conditions (e.g. one sorting cell is run during excitatory conditions and another during inhibitory conditions), after which a final sorting rule can be defined. The module was integrated on an FPGA, within a multichannel processing architecture, and experimental results proved its efficiency on pancreatic islet cultures.

References

[1] I. L. Jones, P. Livi, M. K. Lewandowska, M. Fiscella, B. Roscic, and A. Hierlemann, "The potential of microelectrode arrays and microelectronics for biomedical research and diagnostics," *Anal. Bioanal. Chem.*, vol. 399, no. 7, pp. 2313–2329, Mar. 2011.

[2] M. E. Spira and A. Hai, "Multi-electrode array technologies for neuroscience and cardiology," *Nat. Nanotechnol.*, vol. 8, no. 2, pp. 83–94, 2013.

[3] Y. H.-L. Luo and L. da Cruz, "A review and update on the current status of retinal prostheses (bionic eye)," *Br. Med. Bull.*, vol. 109, no. 1, pp. 31–44, Mar. 2014.

[4] F. Lebreton, A. Pirog, I. Belouah, D. Bosco, T. Berney, P. Meda, Y. Bornat, B. Catargi, S. Renaud, M. Raoux, and J. Lang, "Slow potentials encode intercellular coupling and insulin demand in pancreatic beta cells," *Diabetologia*, pp. 1291–1299, 2015.

[5] E. Pedraza, A. Karajić, M. Raoux, R. Perrier, A. Pirog, F. Lebreton, S. Arbault, J. Gaitan, S. Renaud, A. Kuhn, and J. Lang, "Guiding pancreatic beta cells to target electrodes in a whole-cell biosensor for diabetes," *Lab Chip*, vol. 15, no. 19, pp. 3880–3890, 2015.

[6] R. Biran, D. C. Martin, P. A. Tresco, "Neuronal cell loss accompanies the brain tissue response to chronically implanted silicon microelectrode arrays," *Exp. Neurol.*, vol. 195, no. 1, pp. 115–126, Sep. 2005.